International Journal of Agriculture and Environmental Research

ISSN: 2455-6939

Volume:04, Issue:02 "March-April 2018"

COMPARISON OF SEBAL ESTIMATED HEAT FLUXES AND EVAPOTRANSPIRATION USING FIELD AND REMOTE SENSING DATA IN THE SUDANIAN SAVANNA IN WEST AFRICA

[1]Oluwadare Ayoola O., [1]Okogbue Emmanuel C., [2]Kunstmann Harald, [1]Akinluyi Frank, [2]Arnault Joel, [3]Tayari Salisu, [4]Hingerl Luitpold, [4]Bliefernicht Jan.

[1]Federal University of technology, Akure, Nigeria

[2]Institute of Meteorology and Climate Research, Karlsruhe Institute of Technology (KIT), Germany.

[3]Bolgatanga Polytechnic, Bolgatanga, Ghana

[4]Regional Climate and Hydrology, University of Augsburg, Germany

ABSTRACT

Adequate information on spatial and temporal distribution of surface energy balance components in the sub-Sahara region of West-Africa are critical for sustainable management of water resources besides better understanding of water and heat exchange processes between land surface and atmosphere. this study aim to; estimate surface energy fluxes and evapotranspiration in the Sudanian savannah in West Africa using both Eddy Covariance EC and remote sensing technique, and compare the result from the two techniques. Three EC stations' data installed close to the Ghana–Burkina-Faso border in West Africa were used to determine the surface energy fluxes. SEBAL (Surface Energy Balance Algorithm for Land) model was used to estimate the regional distribution of the surface energy fluxes and evapotranspiration from these sites. When comparison was made between the SEBAL modelled result with data from the EC stations, findings showed relatively good correlation of more than 0.6 from the three stations respectively.

Keywords: Eddy Covariance, Evapotranspiration, Heat Fluxes, Landsat 8, SEBAL

1. INTRODUCTION

The availability and management of water supply in the sub-Sahara region of West-Africa is becoming a great concern. Food production and abundant availability of sustainable agricultural products for the increasing population in the Semi-arid regions of West Africa and changing climate, depends mostly on the good management of water resources. Most farm and agricultural

ISSN: 2455-6939

Volume:04, Issue:02 "March-April 2018"

land has been degraded due to intense human activities, in view of the fact that, farming and livestock rearing is the major occupation of the people living in the area. Thus, comprehensive understanding of water cycle in this region is essential for water resources and agricultural management, as fresh water for human consumption and agricultural purpose is becoming scarce in the arid and semi-arid region of West Africa.

Water from the land surface is continually released to the atmosphere either through evaporation from soils or water bodies or transpiration from vegetation in a process known as evapotranspiration *ET*. It is an important term in the hydrological cycle as it plays a key role in the uptake of water to the atmosphere and returns it back on the earth's surface.

It has been projected that climate change will influence the global water cycle, therefore, intensifying evapotranspiration globally (Huntington 2006, Meehl *et al.* 2007) and consequently leading to the scarcity of water resources (Jung *et al.* 2010).

However, the combination of warmer temperatures with constant or reduced precipitation in other regions may lead to a large decrease in water availability for natural and agricultural systems as well as for human needs, especially in arid or semiarid areas (Jung *et al.* 2010).

Evapotranspiration is represented in the energy balance as the latent heat flux. Adequate information on the spatial and temporal distribution of sensible and latent heat fluxes is critical in many fields, for example, crop management, watershed modelling, and determination of the available water supply. Latent and sensible heat fluxes are subject to rapid changes in time and space. It is extremely difficult to determine their spatial and temporal distributions over large areas from ground measurements alone.

Actual *ET* losses from a watershed cannot be measured directly, it has to be estimated from water budget analysis, such that, the water budget components from the watershed are measured (excluding *ET*) and *ET* is obtained as the residue. ET is measured by instruments such as lysimeters or eddy-covariance (EC) systems, but, these methods are limited in that they provide values of ET at specific sites and not at a regional or larger scale. Moreover, major hydrological variables required for quantifying the availability of water, such as soil moisture, actual evapotranspiration, rainfall and surface runoff are not readily available because measurements of these variables are not performed on a regular basis and most ungauged areas/watershed in West Africa do not have sufficient observation data. As sure, methods have been developed over the years that provide available hydrological data over large areas using remote sensing. These remote sensing (RS) techniques had shown the potential to retrieve distributed and estimates of these parameters at regional and global scales with reasonable accuracy (Droogers and Bastiaanssen 2002; Chen *et al.* 2005; Allen *et al.* 2005, Kalma, et al. 2008).

ISSN: 2455-6939

Volume:04, Issue:02 "March-April 2018"

Furthermore, eddy covariance above-canopy measurement of water vapour flux provides one of the most reliable and widely applied methods for estimating short- and long-term total evapotranspiration (Foken *et al.* 2004). In this technique, great care must still be taken in analysing the EC flux data to account for non-ideal measurement conditions (Massman and Lee 2002, Mahrt, 2010).

The objectives of this study were to; estimate heat fluxes and evapotranspiration in the Sudanian savannah in West Africa using the eddy covariance technique and remote sensing techniques, and compare the result from the two techniques.

2. CLIMATE OF THE STUDY AREA

The entire three sites used in this study are characterised by the Sudanian savanna climate and vegetation. The climate of this region is largely influenced by the movement of the Inter-Tropical Discontinuity (*ITD*) that is, an area of low pressure cells, where the Northeast Trade Winds meet the Southeast Trade Winds over land, near the Earth's equator. In the region, one can distinguish between the dry and dusty air locally referred to as the ‘‘Harmattan’’, which is usually advected from the sahelian areas and the “southwest monsoon”, a moist wind blowing from the Gulf of Guinea. As such, the area is characterized with two seasons (dry and wet season), resulting from the interaction of the two migrating air masses. The dry season begins in the month of November and ends in the month of April. The dry season is dominated by dry and dusty harmattan winds, which is hot during the day and cold during the night. This wind is often accompanied by dust which is responsible for the semi-permanent presence of dry fogs from the month of December to March with concentration of aerosols ranging from 15 to 20 mg cm^3 (Compaore *et al.* 2007), driest months are December and January. The wet season has a mono-modal rainfall distribution pattern, usually from May to October with the rainfall peak occurring in the month of August. The rainfall is erratic and spatial in duration. The onset of the wet season is generally stormy, while the effective rainfall for agriculture purpose is low, due to the high run-off and evaporation (Callo-Concha *et al*. 2012).

The average temperature over the area ranged between 22°C and 40°C in the region, the lowest temperature are experienced in December while the highest temperature occur in March. Annual relative humidity ranged between 6% during the dry season to 95% in the wet season and annual rainfall ranged between 320 and 1100 mm with high spatial and temporal variability.

ISSN: 2455-6939

Volume:04, Issue:02 "March-April 2018"

3. DATA AND METHODOLOGY

3.1 Landsat 8

The Landsat 8 satellite is an earth observation satellite having two sensors, namely, the Operational Land Imager (OLI) and the Thermal Infrared Sensor (TIRS). It measures the visible, near infrared, and short wave infrared portions of the spectrum between 0.433 and 12.5 µm. The two sensors provide seasonal coverage of the global landmass at a spatial resolution of 30 m for the visible, NIR, SWIR bands respectively, 100 m spatial resolution for the thermal bands and 15 m spatial resolution for the panchromatic band. It has a temporal resolution of 16 days. It has a viewing swath width of 185 km, covering wide areas of the earth's landscape, it provide sufficient resolution to be able to distinguish different features on the earth surface like farm, forest, rural areas, urban centres and other land uses. The Spatial and Spectral Characteristics of Landsat 8 can be obtained from the website (http://landsat.usgs.gov/band_designations_landsat_satellites.php).

Ten totally cloud-free Landsat 8 images acquired in 2013 were used. The area of study is located in the path/row 194/53 and 195/52 of Landsat 8 images, available at the USGS cluster. These images were downloaded from http://glovis.usgs.gov. The list of downloaded LANDSAT 8 satellite images used, are given in table 1.

3.2 Eddy Covariance data

Three Eddy Covariance (EC) stations were installed close to the Ghana–Burkina-Faso border in West Africa. The location map of the study area is presented in Figure 1. The first EC station was established in a village called Sumbrungu Aguusi (10.841°N, 0.918°W), elevation 190 m above sea level (ASL) in the Vea catchment, about 35 km drive away from Bolgatanga (a major city) in the Upper East region of Ghana, West Africa. The second EC station was installed in Kayoro Dakorenia (10.918°N, 1.319°W), 292 m above sea level (ASL), within the Tono catchment about 100 km drive from Bolgatanga in the Upper East Region of Ghana, West Africa. The third EC station was installed in Nazinga Park (11.152°N, 1.586°W, 296 m ASL), which is a big natural reserve located about 50 km from Po in the Nahouri province of southern Burkina Faso, West Africa. The EC station is found within the Sissili river basin. The Study sites description can be found in Quansah *et al*. (2015). These EC stations were installed in order to measure the net radiation, sensible, latent, and ground heat fluxes respectively in the sites. The EC Instrumentation, Data acquisition and quality control can be found in both Bliefernicht *et al*. (2013) and Quansah *et al*. (2015).

ISSN: 2455-6939

Volume:04, Issue:02 "March-April 2018"

Table 1: Downloaded LANDSAT 8 satellite images used in this study.

Acquisition date	Day of the year (DOY)	**Path/Row**	Catchment	Stations within the Catchment
18 September 2013	261			
20 October 2013	293			
5 November 2013	309	**194/53**	Vea	Sumbrungu
7 December 2013	341			
11 October 2013	284			
27 October 2013	300		Tono	Kayoro
12 November 2013	316	**195/52**	and	and
28 November 2013	332		partly Sissili	Nazinga Park
14 December 2013	348			
30 December 2013	364			

ISSN: 2455-6939

Volume:04, Issue:02 "March-April 2018"

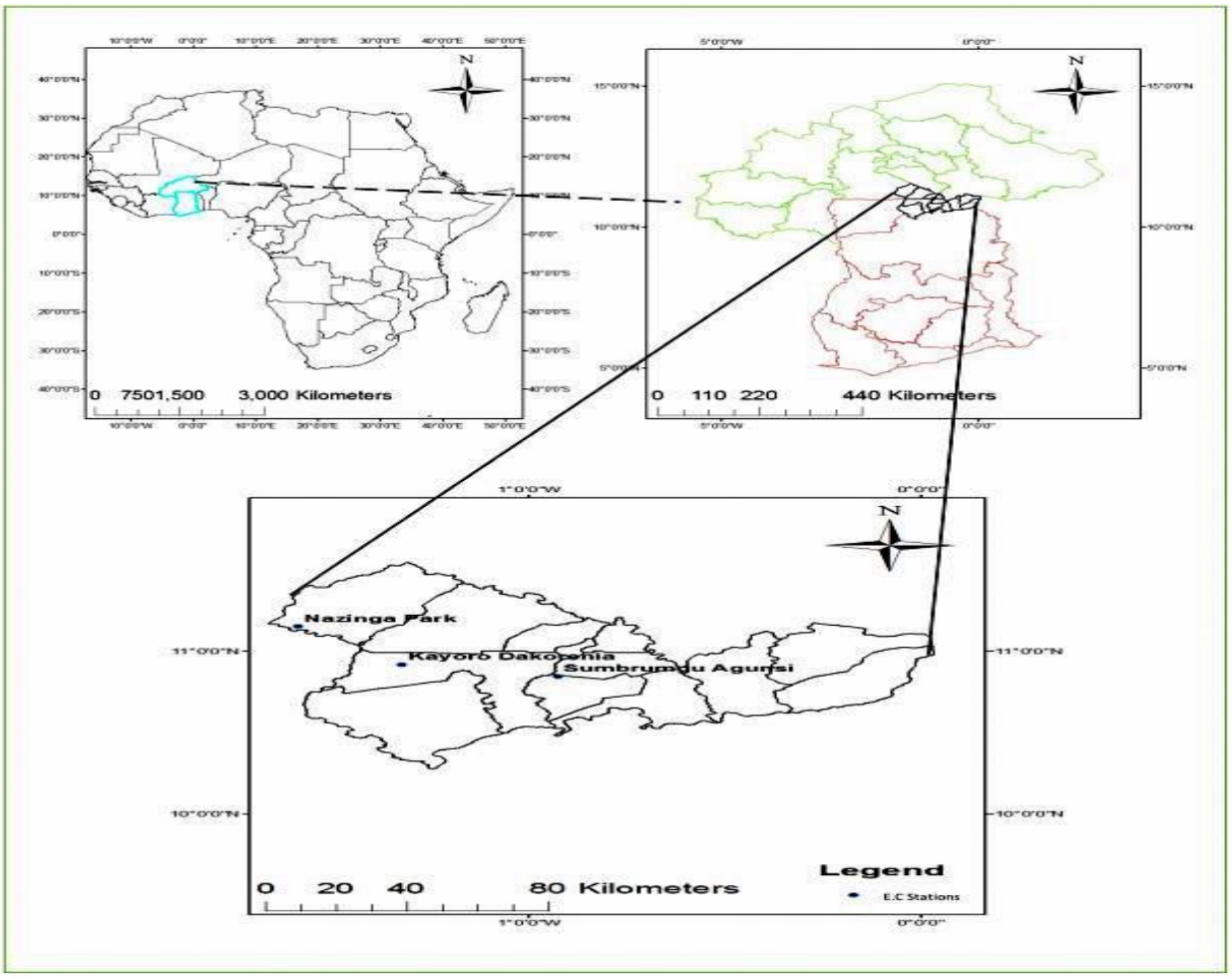

Figure 1: Location map of the study area

3.3 Surface Energy Balance Algorithm for Land (*SEBAL*)

The method used in this study to retrieved surface energy fluxes from remote sensed data is the method proposed by Bastiaanssen *et a*l. (1998) called *SEBAL*. It is a physically based algorithm that requires some ground based variables and remote sensing data in the visible, near infrared and thermal infrared band of the satellite spectral, acquired on a cloud-free day. The model uses physical models to evaluate the net radiation, the resistance for momentum and heat transport, ground heat flux for every individual pixel at the time of satellite overpass, and determines the latent heat flux as the remaining term of the energy budget equation.

$$LE = R_n - G - H \quad (1)$$

ISSN: 2455-6939

Volume:04, Issue:02 "March-April 2018"

where R_n is the net radiation, G is the soil heat flux H is the sensible heat flux and LE is the latent heat flux. The theoretical basis of SEBAL explained in details can be found in Bastiaanssen *et a*l. (1998).

The net radiation (R_n) is computed as the sum of the net shortwave and the net longwave radiation.

$$R_n = (1-\alpha)R_{S\downarrow} + R_{L\downarrow} - R_{L\uparrow} - (1-\varepsilon_o)R_{L\downarrow} \quad (2)$$

where $R_{s\downarrow}$ is the incoming shortwave radiation, $R_{l\downarrow}$ is the incoming longwave radiation which is emitted from the atmosphere , $R_{l\uparrow}$ is the outgoing longwave radiation which is emitted from the land surface, α is the surface albedo and ε is the thermal emissivity of the surface (that is, the degree at which the surface behaves like a perfect blackbody).

The broadband surface albedo (α) was obtained from the top of the atmosphere reflectance at the broadband shortwave (0.25 – 5.0 µm) region of the Landsat 8 data using the semi-empirical relation proposed by Liang (2000).

$$\alpha = 0.356_{\alpha 2} + 0.130_{\alpha 4} + 0.373_{\alpha 5} + 0.085_{\alpha 6} + 0.072_{\alpha 7} - 0.0018 \quad (3)$$

where α_i is the reflectance in spectral band i of the LANDSAT 8 satellite sensor. The bands include the visible bands of 2 and 3, near-infrared of band 5 and the shortwave near-infrared of band 6 and 7 respectively.

The reflectance of each band of LANDSAT 8 was calculated, following the method describe by NASA (landsat.usgs.gov/Landsat8_Using_Product.php 9/4/13). Where, the Digital Number (DN) of each pixel was first converted to spectral radiance and then to reflectance.

The surface temperature was calculated as:

$$T_s = \frac{T_b}{\varepsilon_0^{0.25}} \quad (4)$$

where T_b is the brightness temperature, for Landsat 8, it is given as:

$$T_b = \frac{K_2}{\ln\left(\frac{K_1}{L_\lambda} + 1\right)} \quad (5)$$

ISSN: 2455-6939

Volume:04, Issue:02 "March-April 2018"

L_λ is the spectral radiance of thermal band 10 $\left(Watts/m^2 \times srad \times \mu m\right)$, K1 and K2 are thermal constants. In Landsat 8, K_1 = 774.89 for band 10, while K_2 is 1321.08 for band 10.

The soil heat flux was computed using the empirical equation developed by Bastiaanssen (2000), where G is related to R_n, surface albedo α, surface temperature T_s and normalized difference vegetation index *NDVI* .

$$G = R_n\left[\frac{T_s}{\alpha}\left(0.0032\alpha + 0.0074\alpha^2\right)\right] \times \left(1 - 0.98NDVI^4\right) \quad (6)$$

The sensible heat is the energy transferred between the surface and the atmosphere when there is a temperature difference between them. It can be computed using the bulk aerodynamic method as expressed as

$$H = \frac{\rho_a \times C_p \times dT}{r_{ah}} \quad (7)$$

where ρ_a is the density of air in Kgm^{-3}, C_p is the specific heat capacity of air $\left[1004\ JKg^{-1}K^{-1}\right]$, dT $\left[K\right]$ is the temperature difference between two heights and r_{ah} is the aerodynamic resistance to heat transfer. The instability of atmosphere, due to buoyancy effect of surface heating was corrected in SEBAL by an iteration process (Tasumi and Allen 2000).

The aerodynamic resistance was expressed as a function of surface roughness, wind speed and displacement height;

$$r_{ah} = \frac{\ln\left(z_2/z_1\right)}{u^* k} \quad (8)$$

where z_1 $\left[m\right]$ is the zero plane displacement height, z_2 $\left[m\right]$ is the reference height (The values of *z1* and *z2* was set to constant values of 0.1 and 2.0 m respectively, independent of cover type), k is the von Karman constant $\left(0.4\right)$ and u^* is the friction velocity expressed as

$$u^* = \frac{u(z)k}{\ln\left[z/z_{om}\right]} \quad (9)$$

ISSN: 2455-6939

Volume:04, Issue:02 "March-April 2018"

where $u(z)$ $\left(ms^{-1}\right)$ is the wind speed at reference height z, and z_{om} (m) is the particular momentum roughness length for each pixel given in Tasumi and Allen (2000) as,

$$z_{om} = \exp\left[\left(\frac{c_1 \times NDVI}{\alpha}\right) + c_2\right] \tag{10}$$

where c_1 and c_2 are constants determined for each satellite images.

The temperature difference dT is expressed as

$$dT = \frac{H \times r_{ah}}{\rho_a \times C_p} \tag{11}$$

In order to determine the dT function in SEBAL, two anchor pixels are selected where a reliable value for dT is estimated and H can be predicted. These two pixels selected are the dry and wet pixels. These wet and dry pixels were selected manually in the satellite image. The wet pixel is a pixel that has a low surface temperature and it is assumed that H is approximately equal to zero (i.e. all the available energy [Rn – G] is used to evaporate water from the surface and not to warm the surface) and surface temperature equal to near surface air temperature, that is, $dT = 0$. For this pixel, a well-watered agricultural field was selected, so that the aerodynamic temperature would be similar to that of other vegetative surfaces, such that dT for this wet pixel is assumed to be zero.

For the dry pixel, a dry agricultural surface or a bare soil was selected, having a high surface temperature. The pixel is assumed to have LE approximately equal to zero, so that H can be retrieved from the residual of Rn – G and dT is maximum in this pixel. SEBAL assumes a linear relationship between dT and surface temperature T_s

$$dT = a \cdot T_s + b \tag{12}$$

where a and b are the linear regression coefficients valid for a given satellite image at a particular time. With the known values of T_s and dT as the hot and cold pixel respectively, a and b can then be solved iteratively.

The instantaneous value of the latent heat flux was computed for each pixel using equation (1) at the time of satellite overpass. The instantaneous latent heat flux was then extrapolated to daily

ISSN: 2455-6939

Volume:04, Issue:02 "March-April 2018"

latent heat flux (λET_{24}) using the evaporative fraction (EF) which is assumed to be constant over the day (Brutsaert and Sugita 1992, Farah *et al.* 2004) as:

$$EF_{inst} = \frac{R_n - G - H}{R_n - G} \quad (13)$$

Where, R_n is the instantaneous net radiation and G is the instantaneous ground heat flux.

$$\lambda ET_{24} = EF_{inst} \times \left(Rn_{24} - G_{24} \right) \quad (14)$$

where, G_{24} is the daily ground heat flux which is close to zero, R_{n24} is the daily net radiation.

3.4 Evaluation Criteria

The performance of the model in estimating the energy heat fluxes and ET were quantified based on Coefficient of determination (r^2) and Root Mean Square Error (RMSE)

4. RESULTS AND DISUSSION

4.1 Remote Sensed Estimation of surface fluxes

Using the satellite imageries given in table 1, together with routine meteorological data on air temperature, humidity and wind speed from the EC stations, pixel-based surface fluxes and daily actual ET were computed by solving the surface energy balance for the study area.

In the process of SEBAL ET estimation, net radiation, ground heat, sensible heat and latent heat fluxes were estimated. The estimated fluxes and daily actual ET were in form of maps, such that each pixels contain the estimated value, showing spatial distribution of the fluxes over the study area at 10:30 GMT during satellite overpass. Spatial distribution of fluxes from one of the LANDSAT 8 scenes for 27 October 2013 is presented in figure 2 to figure 5.

NDVI

Figure (2a) shows the NDVI image from one of the LANDSAT 8 scenes at 10:30 GMT for 27 October 2013. Negative values of NDVI correspond to water bodies, Values close to zero (between 0 and 0.1) generally correspond to barren areas of rock or sand. Low positive values represent shrub and grassland which is approximately 0.2 to 0.4, while high values indicate temperate and tropical rainforests with values approaching 1. From the figure, the spatial distribution of red colour on the map represent the areas with lower NDVI values which means,

ISSN: 2455-6939

Volume:04, Issue:02 "March-April 2018"

the area has less or no vegetation. The green parts represent healthier vegetation corresponding to high NDVI values.

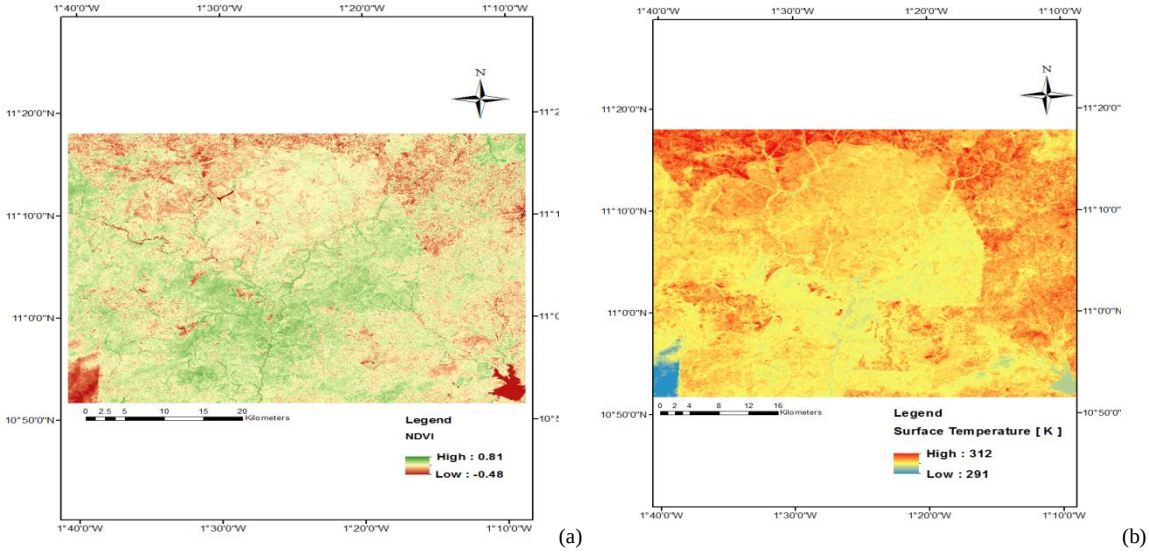

Figure 2: NDVI map (a) and Surface Temperature map (b) from one of the LANDSAT 8 scenes for 27th October 2013.

Surface Temperature

Figure (2b) shows the spatial distribution of surface temperature from one of the LANDSAT 8 scenes at 10:30 GMT for 27 October 2013. The parts with red colours depict the hotter region/surfaces whereas the parts with blue depict the cooler region. The red parts of Figure 2 shows the hot regions and this is typical of land cover type such as desert area, urban/rural areas, and tarred/concrete surfaces, whereas the light blue colour represents cool regions typical of landcover type such as water bodies and healthier vegetated areas. It is also noticeable that the areas with higher surface temperature correspond with area that has low NDVI values. Also, areas with lower surface temperature correspond with areas with has high NDVI values.

Net Radiation

Figure (3a) shows the spatial distribution of net radiation from one of the LANDSAT 8 scenes at 10:30 GMT for 27 October 2013. The three main landscape features can be easily recognized; the desert areas in the upper part of the image have low net radiation values, the natural reserve park in the middle of the image and densed vegetated areas has a relatively high net radiation values. A dam called the Tono dam in the bottom right of the image is also clearly visible with very higher values of net radiation. A similar distribution is found in all scenes.

ISSN: 2455-6939

Volume:04, Issue:02 "March-April 2018"

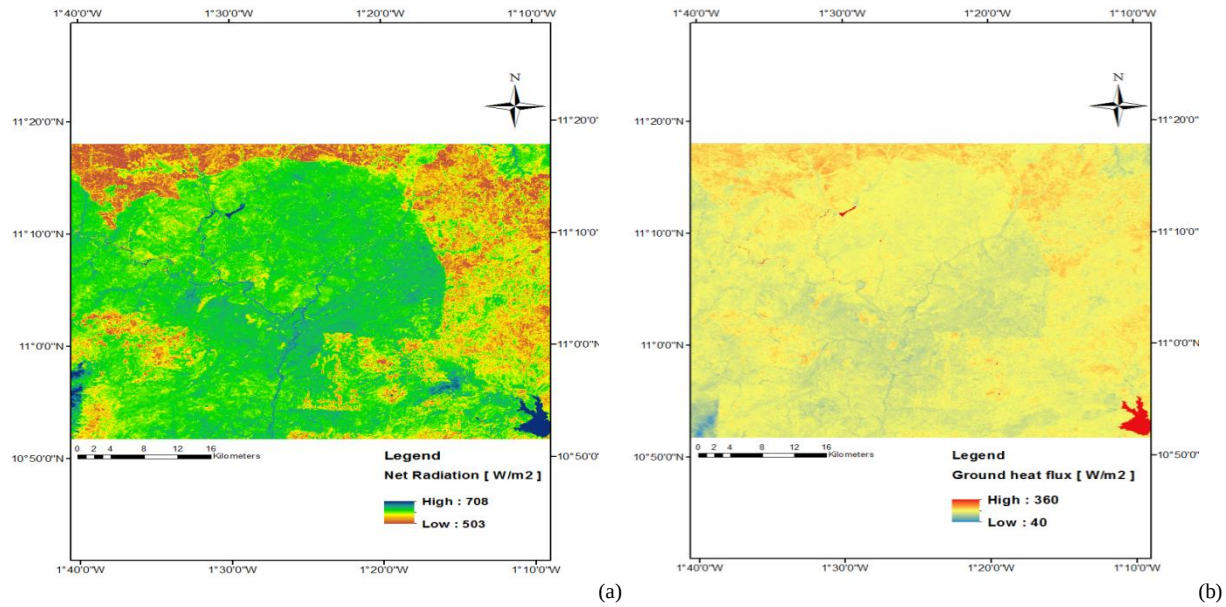

(a) (b)

Figure 3: Spatial distribution of net radiation (a) and Ground heat flux (b) from one of the LANDSAT 8 scenes for 27th October 2013.

Ground Heat Flux

Figure (3b) shows the spatial distribution of Ground heat flux from one of the LANDSAT 8 scenes at 10:30 GMT for 27 October 2013. Spatial distribution of ground heat flux showed that densed vegetated areas, irrigated areas and pixels that falls within the natural reserve park had low values of soil heat flux, pixels that falls within bare soil and desert areas had a higher ground heat flux as compared with the vegetated areas. The water body was found to have the higher value of Ground heat flux. Moreover, similar pattern were found for other scenes.

Sensible Heat Flux

Spatial distribution of the sensible heat flux as shown in figure 4a showed that pixels with higher surface temperature correspond to area with that has the highest values of sensible heat flux found in the desert area, dry and bare soil surface and urban/rural areas, as most of the available energy was used to heat up the surfaces, this was followed with areas with less densed vegetated areas. While the water body and densed vegetation was found to have the lowest value of sensible heat flux. Also, other scenes had similar pattern of the spatial distribution sensible heat flux with respect to land cover type.

ISSN: 2455-6939

Volume:04, Issue:02 "March-April 2018"

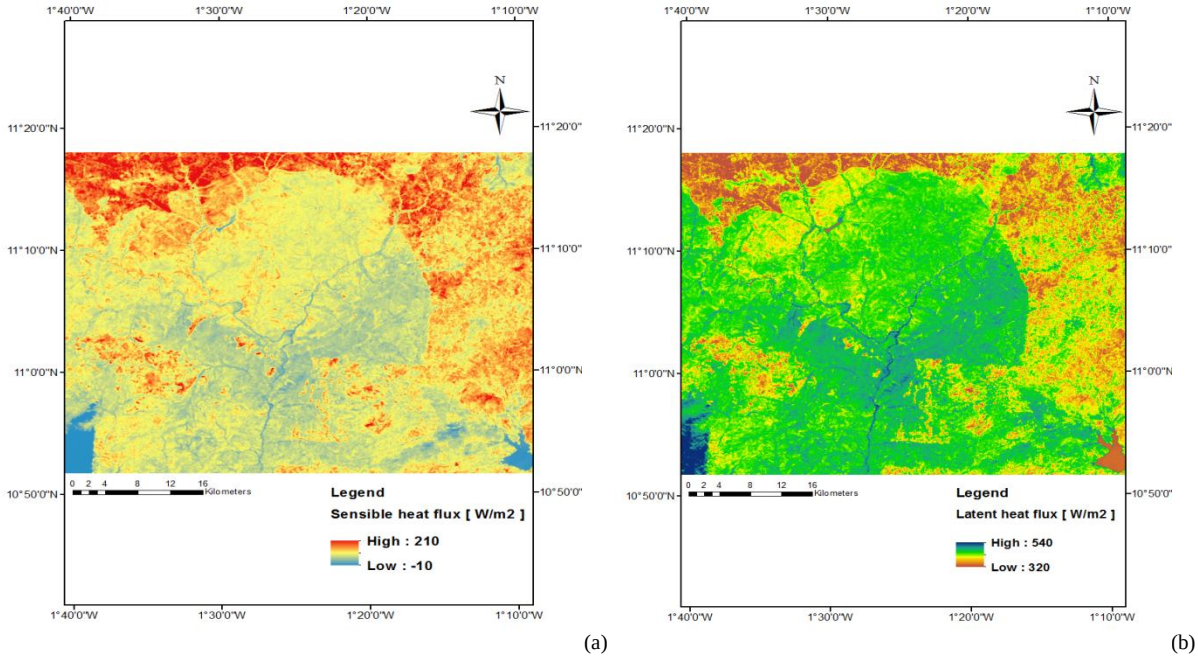

(a) (b)

Figure 4: Spatial distribution of sensible heat flux (a) and Latent heat flux (b) from one of the LANDSAT 8 scenes for 27th October 2013.

Latent Heat Flux and Daily Evapotranspiration

The spatial distribution of latent heat flux across the study area as presented in Figure 4b showed that, the lowest value of latent heat flux was observed across dry and bare soil. It was interesting to note that densed vegetation had higher latent heat flux value that the water bodies. However, the spatial distribution of daily ET as seen in Figure 5, high daily *ET* values were observed along river bed and in the dam of the study area, while low values are observed on the north-eastern sides. This is as a result of differences in land management practices and land cover-types. The north-eastern part is less cultivated and therefore drier compared to the densed vegetated areas (as can be seen in figure 2a). High daily *ET* values were also found in densely vegetated areas within the natural reserve forest. Low daily *ET* values are found in bare land, shrub land and farmland, which are sparsely vegetated area. The study area showed that at this time, the savannah landscape was relatively moist, and most land use type was found to transpire water. However, due to the climatic conditions at the time (last rain recorded prior to the satellite overpass on the 27th of October was recorded on 20th October 2013 in Kayoro station and 15th of October 2013 in Nazinga), the daily *ET* values were relatively high (for this day, the lowest value was 1.0 mm/d and the highest value was 5.2 mm/d) most of the study area contributed to

ISSN: 2455-6939

Volume:04, Issue:02 "March-April 2018"

atmospheric humidity. Similar pattern of daily *ET* map were found for other scenes with respect to land use type.

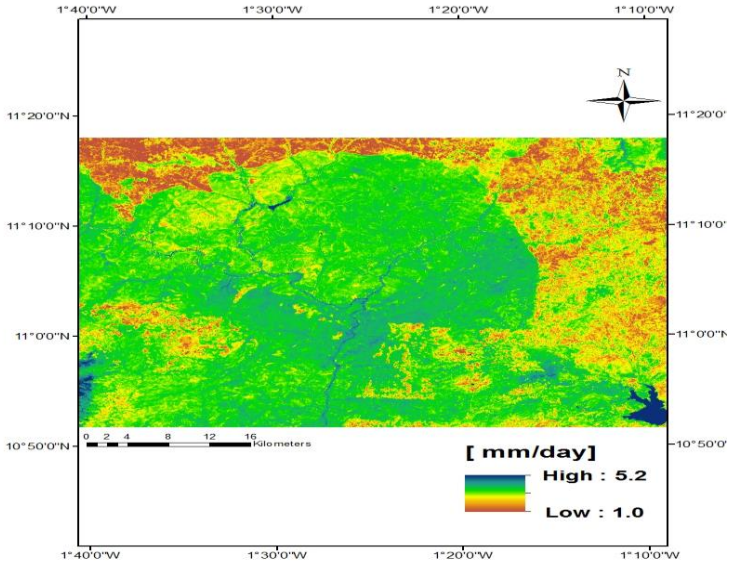

Figure 5: Spatial distribution of daily *ET* from one of the LANDSAT 8 scenes for 27th October 2013.

4.2 Comparison of SEBAL's Instantaneous Energy Fluxes with Ground Measurements

Comparison of SEBAL derived estimates of *Rn, G, H* and *LE* with ground measurements is not a straightforward operation because the spatial and temporal scales of the SEBAL predictions and ground measurements are quite different. For the Kayoro and Nazinga station, six scenes from the LANDSAT 8 were used, while Sumbrungu had four scenes of the LANDSAT 8 that were available for comparison.

4.2.1 Comparison of SEBAL Net Radiation with Ground Measurements

SEBAL estimations for the net radiation and ground heat fluxes were spatially averaged over a 3 × 3 30 m pixels window centred on each EC station, to achieve spatial representativeness of the *in situ* measured fluxes for each sites. Fluxes from six scenes for the area that covers Kayoro and Nazinga station and four scences that covers the Vea catchment where the Sumbrungu Agunsi station is located where compared with the *in situ* measured fluxes.

Figure 6 present the comparisons of the instantaneous *Rn* measured on the ground and that estimated by SEBAL. The method used for the Instantaneous values of Rn derived from SEBAL

ISSN: 2455-6939

Volume:04, Issue:02 "March-April 2018"

at 10:30 GMT satellite over-pass time significantly explained over 90% of the variation of measured values at the Sumbrungu station (r^2 = 0.99), Kayoro station, (r^2 = 0.97), and at the Nazinga station (r^2 = 0.99). The RMSE was 65 W m^{-2} at Sumbrungu, 51 W m^{-2} and 49 W m^{-2} at Kayoro and Nazinga stations respectively.

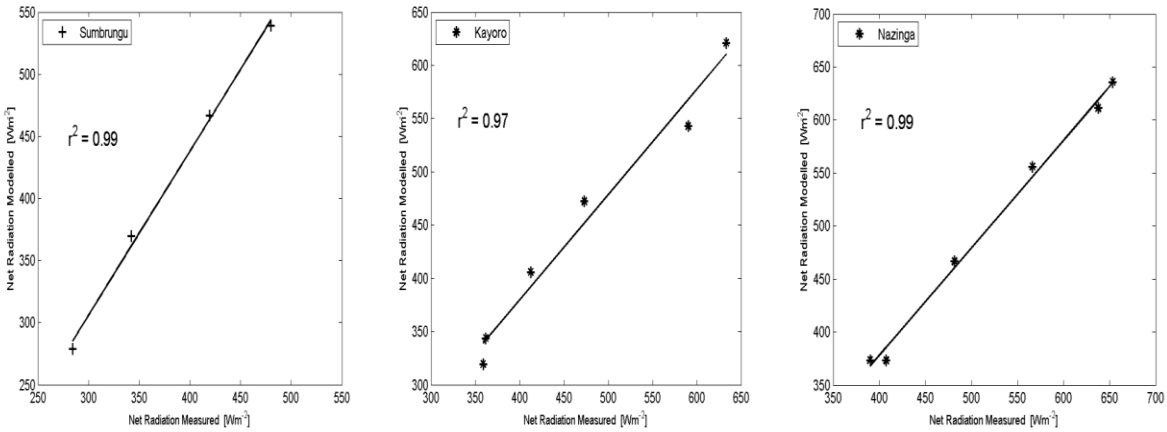

Figure 6: comparison of measured Net radiation at 10:30 and the instantaneous SEBAL estimated values.

4.2.2 Comparison of SEBAL Ground heat flux with Ground Measurements

The ground heat flux *G* was measured by soil heat flux plates combined with the determination of changes in heat storage above the plate using soil temperature and *SWC* measurements. The measurement area of a soil heat flux plate is about 0.001 m^2 which is almost six orders of magnitude less than a 30 × 30 m^2 Landsat pixel (Sauer 2002).

G is spatially variable due to heterogeneity in soil moisture and vegetation cover, so that numerous flux measurements would be needed to estimate the average pixel *G* with the desired accuracy (Humes *et al*. 1994, Kustas and Norman 2000). In most field soils, the instantaneous *G* exhibits not only a temporal variability but also a large spatial variability which makes it very difficult to compare an average *G* for areas with the size of a typical Landsat pixel (Sauer 2002). Given the high spatial and temporal variability of *G*, within one Landsat pixel, the instantaneous measured *G* are expected to be rough estimate of the true instantaneous *G* estimate of a satellite pixel. From Figure 7, Instantaneous values of G at the Sumbrungu station, gave r^2 of 0.27, Kayoro station, (r^2 = 0.03), and at the Nazinga station (r^2 = 0.17). The RMSE was 101 W m^{-2} at Sumbrungu, 31 W m^{-2} at Kayoro station, and 51 W m^{-2} at Nazinga station.

ISSN: 2455-6939

Volume:04, Issue:02 "March-April 2018"

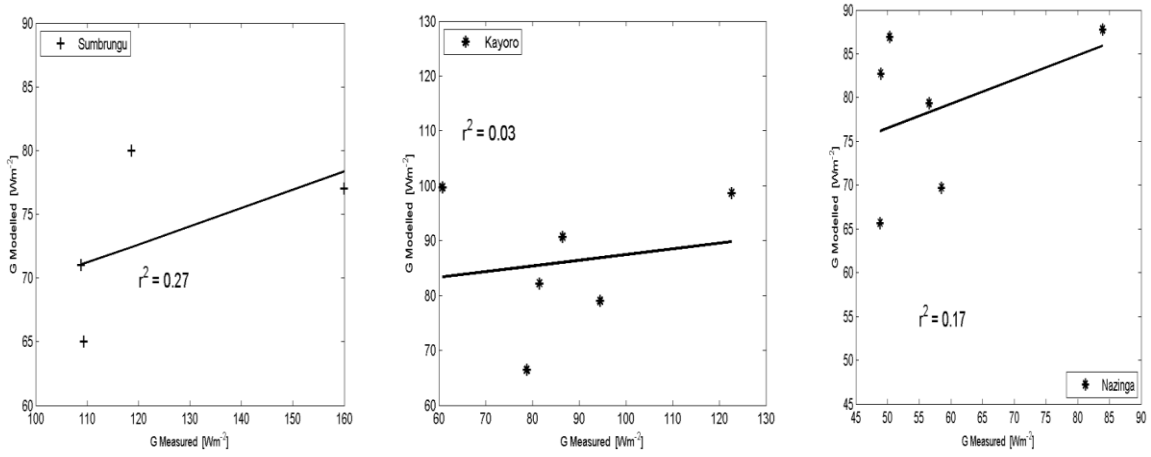

Figure 7: comparison of measured Ground heat flux at 10:30 and the instantaneous SEBAL estimated values.

4.2.3 Comparison of SEBAL Sensible and Latent Heat Fluxes with Ground Measurements

Comparison of SEBAL estimated sensible and latent heat fluxes with ground measurements were done using 3 × 3 30 m pixels window centred on each EC station. The r^2 of the instantaneous flux of H estimated by SEBAL at the Sumbrungu station was 0.64, r^2 = 0.61for the Kayoro station, whilst r^2 = 0.83 for the Nazinga station when comparing the values of SEBAL modelled H with the *in situ* EC measurements (Figure 8). The RMSE of 38 W m^{-2} and 36 W m^{-2} were found for Sumbrungu and Kayoro stations respectively. While a RMSE of 43 W m^{-2} was found for Nazinga station. However similar results were found by other studies (Zhan et al. 1996, Ferguson *et al.* 2010, Teixeira 2010) when validating different models for turbulent flux estimation under different conditions of land use and land cover. At Sumbrungu station, r^2 = 0.83 with a RMSE of 118 W m^{-2}, at Kayoro station, r^2 = 0.87 with a RMSE of 116 W m^{-2}, likewise, r^2 = 0.86 was found for Nazinga station, with a RMSE of 134 W m^{-2}, when comparing SEBAL modelled LE values with the *in situ* EC measurements (Figure 9).

ISSN: 2455-6939

Volume:04, Issue:02 "March-April 2018"

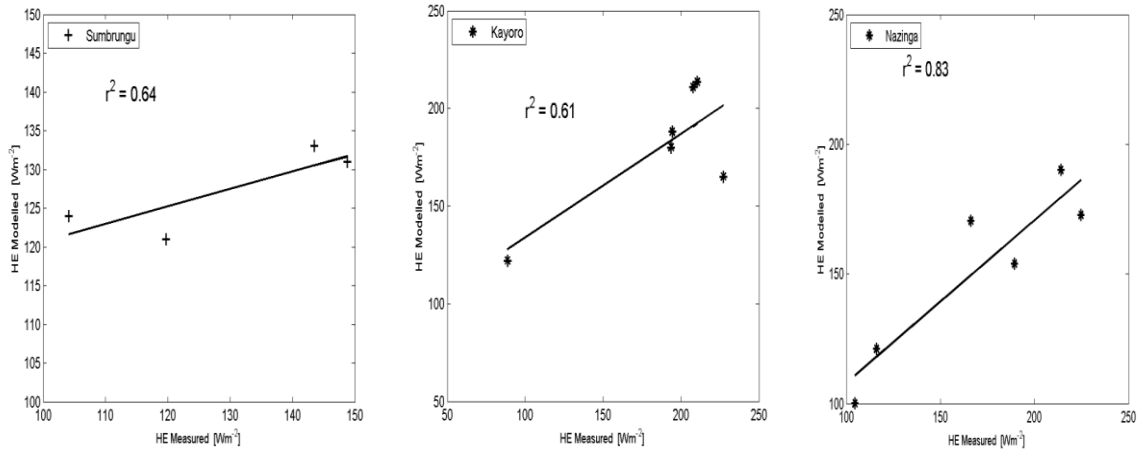

Figure 8: comparison of measured Sensible heat flux at 10:30 and the instantaneous SEBAL estimated values.

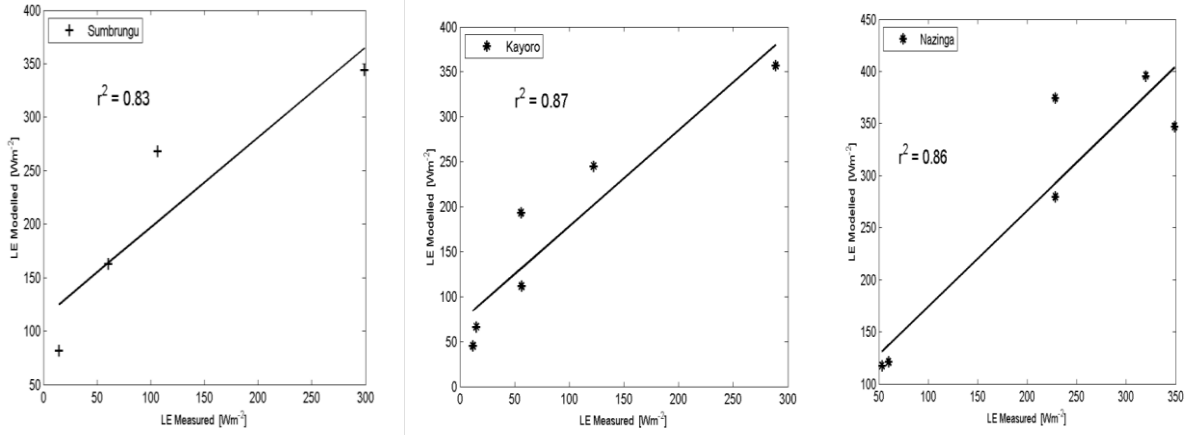

Figure 9: comparison of measured Latent heat flux at 10:30 and the instantaneous SEBAL estimated values.

4.3 Comparison of SEBAL Estimated daily ET from LANDSAT 8 with Ground Measurements

The SEBAL algorithm applied to the different Landsat images (in table 1) using the empirical relationships based on field measurements to estimate the daily *ET* are validated with field measurements from the Sumbrungu, Kayoro and Nazinga station respectively. At Sumbrungu station, the coefficient of determination r^2 = 0.83 with a RMSE of 1.2 mm/d, at Kayoro station, r^2 = 0.77 with a RMSE of 2.4 mm/d, likewise, r^2 = 0.77 was found for Nazinga station, with a RMSE of 1.1 mm/d (Figure 10). The *RMSE* observed for the daily *ET* are quite high, especially

ISSN: 2455-6939

Volume:04, Issue:02 "March-April 2018"

for the Karoyo station. However, according to Bastiaanssen et al. (2008), the values of daily *ET* predicted by the *SEBAL* model are within several percent from the measured values. Considering the fact that, the field measurements have their own sources of errors.

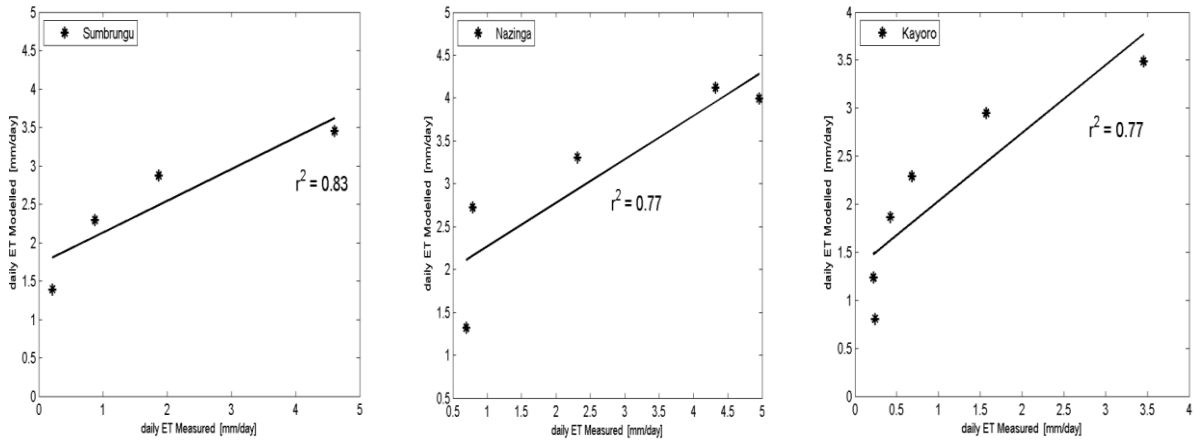

Figure 10: comparison of measured daily *ET* and SEBAL estimated daily *ET* values for Sumbrungu, Kayoro and Nazinga Park respectively.

Nevertheless, this result agrees well with other research done (Bastiaanssen, 2002, Mohamed *et al.* 2004, Compaoré *et al.* 2007, Opoku-Duah *et al.* 2008, Teixeira *et al.* 2009, Jia *et al.* 2013, Kiptala *et al.* 2013) that the SEBAL model can be used in estimating the spatial distribution of daily ET over a watershed using satellite data.

5. CONCLUSION

The spatial distribution of the net radiation, Ground heat flux, sensible heat flux and latent heat flux changes with respect to different land use /land cover type. For the daily *ET*, lowest daily *ET* values was observed in bare soil and dry farmland and increases in wetlands/ dense vegetated area and in the forest region. The highest daily ET values were however, observed in water bodies.

To complement the finding of the spatial distribution of energy fluxes using the remote sensing algorithm, the comparison between the measured energy fluxes and that estimated from SEBAL was done. At the stations, instantaneous net radiation estimated from SEBAL, when compared to the measured values were found to be much more similar with r^2 of 0.99, 0.97 and 0.99 at the station in Sumbrungu, Kayoro and Nazinga respectively. Instantaneous fluxes of H and LE estimated by SEBAL had r^2 of 0.62, 0.61 and 0.83 for the sensible heat flux, while the LE had r^2 of 0.83, 0.76 and 0.68 at the Sumbrungu, Kayoro and Nazinga station respectively when

ISSN: 2455-6939

Volume:04, Issue:02 "March-April 2018"

comparing modelled values with the in situ EC measurements. However, the ground heat flux was not properly represented by the satellite data having r^2 of 0.03, 0.03 and 0.17 at the station in Sumbrungu, Kayoro and Nazinga respectively when compared to ground measurement. The difference in the measured and modelled ground heat flux could be as a result of large spatial variability in ground heat flux which makes it very difficult to compare an average ground heat flux for areas with the size of a satellite pixel like LANDSAT. The comparison between the measured and estimated daily *ET* (using the LANDSAT 8 data) gave r^2 of 0.83, 0.77 and 0.77 for Sumbrungu, Kayoro and Nazinga station respectively. The presented results, obtained from the SEBAL algorithm confirm the potential of providing spatial surface energy fluxes and daily ET on clear-sky days over large areas. It also show the potential of remote sense estimated surface energy fluxes and daily *ET* to overcome lack of reliable, objective, exhaustive, and consistent information on the water management problems over West Africa at a regional scale. In a situation where there are insufficient in situ observations and less meteorological stations network that can give better description of the climate variability of a region and validate climate model predictions, evapotranspiration modelled from remote sensing *data* using the SEBAL algorithm could be an alternative in providing decision support for system-wide operational water management issues.

ACKNOWLEDGEMENTS

This work was part of the West African Science Service Centre on Climate Change and Adapted Land Use (WASCAL) funded by the German Federal Ministry of Education and Research (BMBF). We acknowledge the financial support from BMBF for the installation and maintenance of the EC and automatic weather stations at the study areas.

REFERENCES

Allen, R., Pereira, L.A., Raes, D., and Smith, M. (1998). Crop evapotranspiration guidelines for computing crop water requirements. *FAO Irrigation and Drainage* Paper No. 56, FAO, Rome.

Allen, R.G. Tasumi, M. and Trezza. R. (2005). METRIC Mapping Evapotranspiration at High Resolution. *Applications Manual for Landsat Satellite Imagery.* Version 2.0, Kimberly, Idaho, University of Idaho.

Arya, S. P (2001). *Introduction to Micrometeorology*. Second Edition, Academic Press Inc., San Diego, 227 pp.

Bastiaanssen, W.G.M. (2000). SEBAL-Based Sensible and Latent Heat Fluxes in the Irrigated Gediz Basin, Turkey.*J. Hydrol*., 229, 87-100.

Bastiaanssen, W.G.M., Ahmad, M.-D. and Chemin, Y. (2002). Satellite surveillance of evaporative depletion across the Indus Basin. *Water Resources Research* 38:1273, (doi:10.1029/2001WR000386).

Bastiaanssen, W.G.M., Menenti, C., Feddes R.A., and Holtslag A.A.M. (1998). A remote sensing surface energy balance algorithm for land (SEBAL). Part I Formulation. *Journal of Hydrology*, 213 (1-4), 198-212.

Bastiaanssen, W.G.M., Noordman, E.J.M., Pelgrum, H., Davids, G., and Allen, R.G. (2005). SEBAL for spatially distributed ET under actual management and growing conditions, *ASCE Journal of Irrigation and Drainage Engineering* 131(1), 85–93.

Bastiaanssen, W.G.M., Pelgrum, H., Soppe, R.W.O., Allen, R.G., Thoreson, B.P., Teixeira, A.H. de C. (2008). Thermal infrared technology for local and regional scale irrigation analysis in horticultural systems. ISHS Acta Hort. 792.In: Proc. Vth IS on Irrigation of Horticultural Crops.

Bliefernicht Jan, Harald Kunstmann, Luitpold Hingerl, Thomas Rummler, Sabine Andresen, Matthias Mauder, Rainer Steinbrecher, René Frieß, David Gochis, Ursula Gessner, Emmanuel Quansah, Ayoola Awotuse, Frank Neidl, Carsten Jahn and Boubacar Barry (2013). Field and simulation experiments for investigating regional land–atmosphere interactions in West Africa: experimental set-up and first results. Climate and Land Surface Changes in Hydrology, IAHS Publ. 359.

Brutsaert, W., and Sugita, M. (1992). Application of self-preservation in the diurnal evolution of the surface energy budget to determine daily evaporation. *Journal of Geophysical Research* 97. 377-382.

Callo-Concha, D., Gaiser, T. and Ewert, F. (2012). Farming and cropping systems in the West African Sudanian Savanna. WASCAL research area: Northern Ghana, Southwest Burkina Faso and Northern Benin. ZEF Working Paper 100. Bonn. 48 pp.

Chen, J.M., Chen, X., Ju,W. and Geng, X. (2005). Distributed hydrological model for mapping evapotranspiration using remote sensing inputs. *Journal of Hydrology* 305.15-39.

Compaore, H., Hendrickx, J.M.H., Hong, S-h., **Friesen, J.**, van de Giesen, N.C., Rodgers, C., Szarzynski, J. and Vlek, P.L.G. (2007). Evaporation mapping at two scales using optical imagery in the White Volta Basin, Upper East Ghana. Physics and Chemistry of the Earth 33:127-140.

Der Wal, T. (1998). A remote sensing surface energy balance algorithm for land (SEBAL). Part II Validation. *Journal of Hydrology*, 213(1-4). 213–229. (doi: 10.1007/s10795-007-9029-z).

Droogers, P., and Bastiaanssen, W.G.M. (2002). Irrigation performance using hygrological and remote sensing modelling. *Journal of Irrigation and Drainage Engineering* 128.11-18.

Farah, H.O., Bastiaanssen, W.G.M., and Feddes, R.A. (2004). Evaluation of the temporal variability of the evaporative fraction in a tropical watershed, *International Journal of Applied Earth Observation and Geoinformation* 5: 129-140.

Ferguson, C.R., Wood, E.F., Sheffield, J. And Gao, H. (2010). Quantifying uncertainty in a Remote sensing-based estimate of evapotranspiration over continental USA. *Int. J. Remote Sens.*, *31*, 3821-3865.

Foken, T., Göckede, M., Mauder, M., Mahrt, L., Amiro, B. and Munger, W. (2004). *Post-field data quality control. Handbook of Micrometeorology. A guide for surface flux measurement and analysis*. Kluwer Acad. Publ., Dordrecht, the Netherlands, 181–208.

Hendrickx, J.M.H and Hong S.H. (2005). Mapping sensible and latent heat fluxes in arid areas using optical imagery. *Proceedings of International Society for Optical Engineering*, SPIE 5811.138-146.

Humes, K.S., Kustas,W.P., Moran,M.S., Nichols,W.D. and Weltz,M.A. (1994). Variability of emissivity and surface temperature over a sparsely vegetated surface. *Water Resources Research* 30:1299 - 1310.

Huntington, T., (2006). Evidence for intensification of the global water cycle: review and synthesis. Journal of Hydrology, 319, pp. 83–95.

Jensen M.E., Burman R.D. and Allen R.G. (1990). *Evapotranspiration and Irrigation Water Requirements*. Publication 70, American Society of Civil Engineers: New York; 332.

Jia D., Kaishan S., Zongming W., Bai Z. and Dianwei L. (2013). Evapotranspiration estimation based on MODIS products and surface energy balance algorithms for land (SEBAL) model in Sanjiang Plain, Northeast China. *Chinese Geographical Science* 23, 73-91.

Jung, M., Reichstein, M., Ciais, P., Seneviratne, S. I., Sheffield, J., Goulden, M. L., Bonan, G., Cescatti, A., Chen, J., Jeu, R., Dolman, A. J., Eugster, W., Gerten, D., Gianelle, D., Gobron, N., Heinke, J., Kimball, J., Law, B. E., Montagnani, L., Mu, Q., Mueller, B., Oleson, K.,Papale, D., Richardson, A. D., Roupsard, O., Running, S., Tomelleri, E., Viovy, N., Weber, U., Williams, C., Wood, E., Zaehle, S., and Zhang, K. (2010). Recent decline in the global land evapotranspiration trend due to limited moisture supply. Nature 467.951–4

Kalma, J.D., McVicar, T.R. and McCabe, M.F. (2008) Estimating land surface evaporation: A review of methods using remotely sensed surface temperature data. Surveys in Geophysics. 29(4-5), 421-469. doi:10.1007/s10712-008-9037-z.

Kiptala, J. K., Mohamed, Y., Mul M. L. and Van der Zaag P. (2013). Mapping evapotranspiration trends using MODIS and SEBAL model in a data scarce and heterogeneous landscape in Eastern Africa. *Water Resources Research*, VOL. 49, 8495–8510. doi.10.1002/2013WR014240.2013.

Kustas, W. P. and Norman, J. M. (2000). A two-source energy balance approach using directional radiometric temperature observations for sparse canopy covered surfaces, Agron. J., 92, 847–854.

Liang, S. (2000). Narrowband to broadband conversions of land surface albedo I algorithms. *Remote Sensing of Environment* 76, 213-238.

Mahrt, L. (2010). Computing turbulent fluxes near the surface; Needed improvements. *Agric. For. Meteorol.*150. 501–509.

Massman, W. J. and Lee, X. (2002). Eddy Covariance Flux Corrections and Uncertainties in Long Term Studies of Carbon and Energy Exchange. *Agric. For. Meteorol*. 113, 121–144.

Meehl, G. A., Arblaster, J. M. and Tebaldi C. (2007). Contributions of natural and anthropogenic

forcing to changes in temperature extremes over the U.S., *Geophys. Res. Lett.*, 34, L19709, doi.10.1029/2007GL030948

Mohamed, Y.A., Bastiaanssen, W.G.M. and Savenije, H.H.G. (2004). Spatial variability of evaporation and moisture storage in the swamps of the upper Nile studied by remote sensing techniques. *J. Hydrol*. 289 (1–4), 145–164.

Opoku-Duah, S., Donoghue, D. N. M. and Burt, T. P. (2008). Intercomparison of evapotranspiration over the Savannah Volta Basin in West Africa using remote sensing data. Sensors, vol. 8, pp. 2736–2761.

Quansah, E., Mauder, M., Balogun, A. A., Amekudzi, L. K., Hingerl, L., Bliefernicht, J., and Kunstmann, H., (2015). Carbon dioxide fluxes from contrasting ecosystems in the Sudanian Savanna in West Africa. Carbon Balance and Management, 10(1):1 – 17. doi 10.1186/s13021-014-0011-4.

ISSN: 2455-6939

Volume:04, Issue:02 "March-April 2018"

Sanchez, J.M., Scavone, G., Caselles, V., Valor, E., Copertino, V.A., Telesca, V. (2008). Monitoring daily evapotranspiration at a regional scale from Landsat-TM and ETM+ data: application to the Basilicata region. *J. Hydrol*., *351*, 58–70.

Sauer, T.J. (2002). *Soil Heat Flux. Encyclopedia of Soil Science* Marcel Dekker, INC., New York, NY. pp 814 – 816.

Tasumi, M., Allen, R.G., and Bastiaanssen, W.G.M. (2000). The theoretical basis of SEBAL. *Application of the SEBAL methodology for estimating consumptive use of water and stream flow depletion in the Bear River Basin of Idaho through remote sensing*. Final report submitted to the Raytheon Systems Company, Earth Observation System Data and Information System Project. pp 46 - 69.

Teixeira, A.H.C. (2010). Determining regional actual evapotranspiration of irrigated crops and natural vegetation in the São Francisco River Basin (Brazil) using remote sensing and Penman-Monteith Equation. *Remote Sens. 2*, 1287-1319.

Teixeira, A.H.D.C., Bastiaanssen, W.G.M., Ahmadd, M.D. and Bos, M.G. (2009). Reviewing SEBAL input parameters for assessing evapotranspiration and water productivity for the Low-Middle São Francisco River basin, Brazil Part A. *Application to the regional scale*. *Agric. For. Meteorol*. 149, 462-476.

Zhan, X., Kustas, W.P. and Humes, K. (1996). An intercomparison study on models of sensible heat flux over partial canopy surfaces with remotely sensed surface temperature. *Remote Sens. Environ*, *58*, 242-256.

